17

Imaging and Probing Cell Mechanical Properties With the Atomic Force Microscope

Kevin D. Costa

Summary

This chapter describes the use of the atomic force microscope (AFM) to probe and map out regional variations in apparent elastic properties of living cells. The importance of mechanics in the field of cell biology is becoming more widely appreciated, and the AFM has unique advantages for cell mechanics applications. However, care must be taken in the acquisition, analysis, and interpretation of AFM indentation data. To help make this powerful technique accessible to a broad range of investigators, detailed procedures are provided for all stages of the AFM experiment from sample preparation through data analysis and visualization.

Key Words: AFM; scanning probe microscope; nanoindentation; elastography; micromechanics; elastic modulus; stiffness; viscoelasticity; cytoskeleton.

1. Introduction

1.1. Role of Mechanics in Cell Biology

The cell is the basic building block of all living organisms. Every tissue in the body is comprised of cells, and the specialized function of various tissues and organs is fundamentally related to differences in mechano-electro-chemical characteristics of the individual constituent cells and their organization within the tissues. Cell mechanics deals with the mechanical properties and functions of cells *(1)*, including how such properties relate to individual components of the internal cytoskeleton *(2–5)*, how cells respond to external mechanical stimulation *(6–8)*, and how they, in turn, remodel and alter the extracellular matrix *(9–12)*. Indeed, many fundamental aspects of cellular function, including shape, deformability, motility, division, and adhesion, are critically dependent on the mechanical properties (e.g., stiffness, nonlinearity, anisotropy, and heterogeneity) of the cell. There is also growing evidence that

From: *Methods in Molecular Biology, vol. 319: Cell Imaging Techniques: Methods and Protocols*
Edited by: D. J. Taatjes and B. T. Mossman © Humana Press Inc., Totowa, NJ

the state of health or disease of a cell might be detectable as changes in cell mechanical properties *(13)*.

Although micropipet aspiration has become an established method for characterizing the mechanical properties of cells floating in suspension *(14–18)*, a number of alternative techniques (including magnetic twisting cytometry *(19)*, laser tracking microrheology *(20)*, magnetic tweezers *(21)*, the optical stretcher *(22)*, and various cell indenters *(23–25)* have been developed to study mechanical properties of adherent cells with a well-defined cytoskeleton. In particular, following its invention in 1986 as a high-resolution imaging tool *(26)*, the atomic force microscope (AFM) has rapidly become a popular method for studying mechanical properties of living cells in culture *(13,27)*.

1.2. Principle of Operation of AFM

The AFM is well suited for cell mechanics applications because of its high sensitivity (subnanonewton), high spatial resolution (submicrometer), and the ability to be used for real-time measurements in a physiologic aqueous cell culture environment. An important advantage of AFM over other cell mechanics techniques is the ability to combine high-resolution scanning with nano-indentation, which allows direct correlation of local mechanical properties with underlying cytoskeletal structures *(4,28)*. Furthermore, commercial availability of the AFM makes it accessible to a broad range of investigators.

In principle, the AFM is a relatively simple instrument that involves laser tracking of the deflection of a microscopic cantilever probe as its tip scans, indents, or otherwise interacts with the cell (*see* **Fig. 1**). The AFM probe is the transducer of the instrument and typically consists of a rectangular or V-shaped cantilever beam about 100–300 μm long and about 0.5 μm thick, microfabricated of silicon or silicon nitride (*see* **Fig. 2**). The standard AFM probe has an integrated pyramid-shaped tip with a blunted point having a radius of curvature in the 50- to 100-nm range. It is this tip that physically contacts the cell, whereas the cantilever serves as a soft spring to measure the contact force. The AFM sensor uses a laser beam reflected off the end of the cantilever probe and onto a four-quadrant photodetector to monitor vertical and lateral deflections of the probe due to forces at the tip. The distance between the probe and the photodetector amplifies the reflected laser motion such that movements of the AFM tip on the order of 0.1 nm can be reliably detected *(29)*.

The actuator that moves the AFM probe relative to the sample is a piezoelectric ceramic that deforms in response to applied voltages. The typical z-range is about 6 μm, although custom configurations have achieved a z-range up to about 20 μm to better accommodate irregular biological samples *(30)*. Piezoelectric positioners

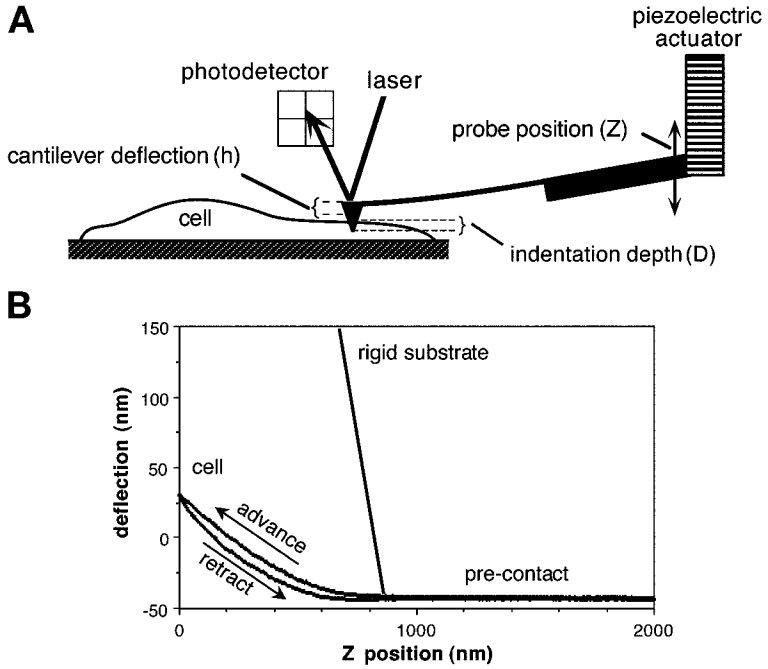

Fig. 1. Schematic of AFM cell indentation experiment. **(A)** Deflection of the AFM cantilever probe is sensed from the reflection of a laser onto a four-quadrant photodetector, and the position of the probe is controlled by a piezoelectric ceramic actuator. As the probe approaches and eventually contacts the cell, further changes in probe position, *Z*, result in a combination of cantilever deflection, *h*, and cell indentation, *D*, dependent on the spring constant of the probe, the geometry of the tip, and the mechanical properties of the cell. **(B)** The resulting measurements of cantilever deflection vs probe position during advancement and retraction of the probe yield the so-called "force curve." On a rigid substrate, the force curve has a linear postcontact region, whereas on a soft sample such as a cell, the postcontact region is more complex.

are used to control movement in the *x*-*y*-plane as well, with a maximum scan range typically around 100 × 100 μm. Although piezoelectric materials are inherently nonlinear and hysteretic, these effects can be overcome by software compensation (open-loop design) or direct strain-gage monitoring (closed-loop design) for precise positioning of the AFM tip. In the standard AFM configuration, the sample is moved relative to a stationary probe. However, for cell biology applications, it is more convenient to place the entire AFM on the stage of an inverted light microscope to allow simultaneous visualization, including fluorescence microscopy, of the cells *(30)*. In this configuration, the AFM probe is moved relative to a stationary sample.

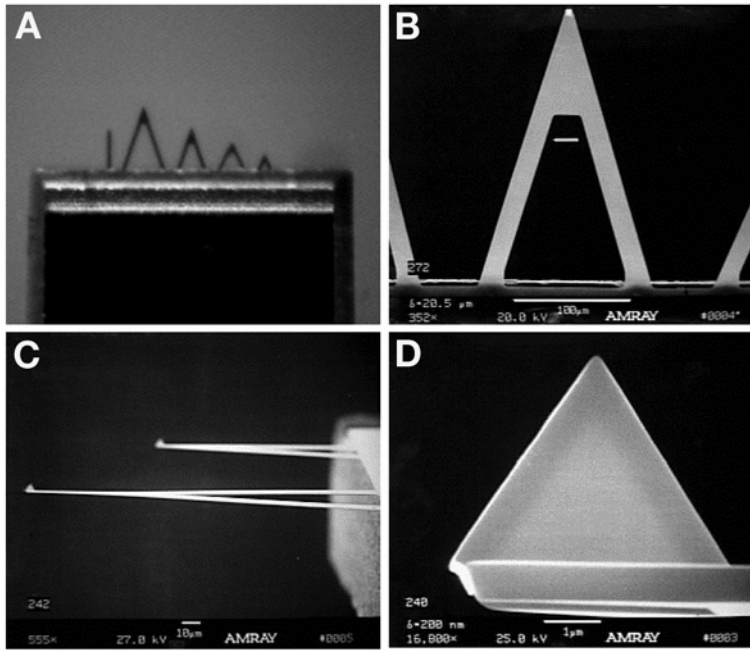

Fig. 2. **(A)** Bright-field image of silicon nitride Microlever® probes on a chip. **(B–D)** Scanning electron microscope images of various AFM probes with standard, unsharpened, integrated pyramidal tips. Scale bars: 100 µm **(B)**, 10 µm **(C)**, 1 µm **(D)**.

The standard AFM controller allows the tip to be raster-scanned over the surface of the cell while monitoring the tip deflection, yielding a high-resolution image of the cell topography. It is also possible to extend and retract the probe perpendicular to the cell surface, thus performing a nano-indentation experiment that can be used to measure the contact force and extract cell mechanical properties.

1.3. Overview

As a wide variety of studies demonstrate *(4,28,31–36)*, the AFM can provide novel information relating cellular structure, mechanical properties, and functions. To help make such tests accessible to a broad range of investigators, this chapter focuses on procedures required to prepare cells for AFM analysis, to characterize the AFM probe, to conduct the AFM indentation experiment, and to analyze and visualize the resulting data. The recent method of analyzing AFM indentation data to extract a pointwise apparent modulus *(37)* is highlighted. As the AFM continues to be developed for cell mechanics applications, other testing procedures and methods of analysis might emerge *(28,38,39)*, but the standard indentation experiment is likely to remain an important protocol for characterizing cell material properties.

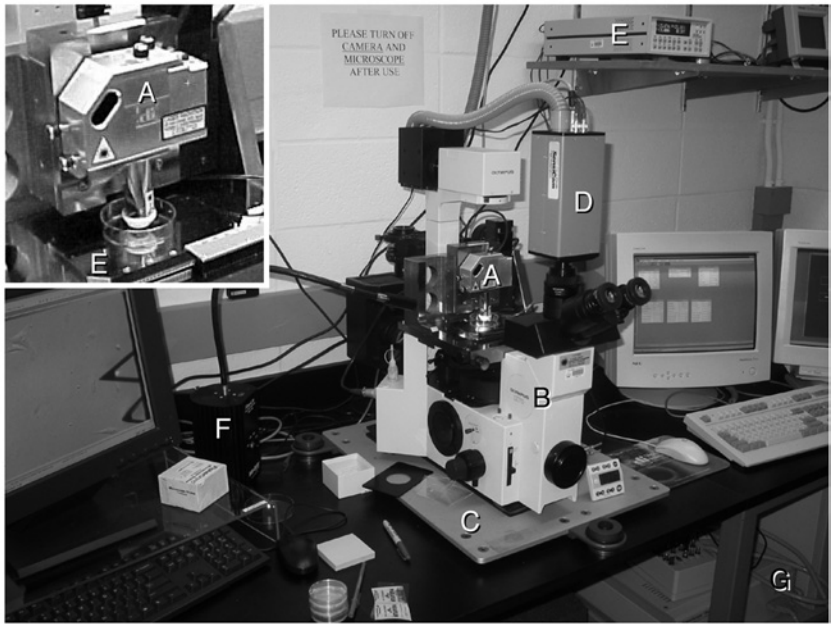

Fig. 3. Typical AFM setup for cell biology applications includes **(A)** AFM scanner housing the laser, photodetector, and piezoelectric actuator, with the cantilever probe mounted at the end exposed to the Petri dish contents, **(B)** inverted light microscope with custom stage, **(C)** vibration isolation platform, **(D)** cooled charge-coupled device camera with vacuum hose leading to remote fan, **(E)** fluid sample heater and controller, **(F)** fiberoptic lamp, and **(G)** AFM controller electronics and computer.

The AFM setup used in the author's laboratory and described herein is a Bioscope® from Digital Instruments (Veeco Metrology Group, Santa Barbara, CA), and a number of accessories and options were also obtained from Digital Instruments for compatibility and convenience (*see* **Fig. 3** and **Note 1**). However, the materials and methods detailed below are intended to apply to any AFM that can be used in a fluid environment to study living cells in monolayer cultures.

2. Materials

2.1. Cell Culture

Beyond the standard solutions and materials used for culturing the cell types of interest, there are two specially recommended cell culture supplies.

1. Gibco CO_2-independent medium (cat. no. 18045, Invitrogen Corp, Carlsbad, CA) supplemented with 4 m*M* L-glutamine according to the manufacturer's instructions (*see* **Note 2**).

2. A 60 × 15-mm polystyrene tissue culture dish (cat. no. 353002, Becton Dickinson, Franklin Lakes, NJ) or other small open-top culture substrate of comparable stiffness that fits under the AFM scanner.

2.2. Probe Setup and Characterization

1. Low-power (40× to 80× max) dissecting microscope (e.g., model SZ-60, Olympus, Woodbury, NY) with external light source.
2. Several microscopic, flat-tipped, stainless-steel tweezers, such as EREM's broad straight tip (cat. no. 2ASA), fine straight tip (cat. no. 3CSA), and 10° offset tip (cat. no. 5ASA), available from Cooper Hand Tools (Raleigh, NC).
3. 30G Hypodermic needles (cat. no. 305128, Becton Dickinson) and 3-mL disposable syringes (cat. no. 309585, Becton Dickinson).
4. Cotton-tipped swabs (cat. no. 14-960-3N, Fisher Scientific, Pittsburgh, PA) and small delicate task Kimwipes® (cat. no. 06-666, Fisher).
5. Glass microscope slides (e.g., cat. no. 12-550C, Fisher) or mica sheets (cat. no. 56, Ted Pella, Redding, CA).
6. Bottled compressed air duster (e.g., cat. no. 23-022523, Fisher).
7. Double-sided cellophane tape (Scotch 137, 3M Corp.) and small Post-it® notes (cat. no. 653, 3M Corp.).
8. Unsharpened, gold-coated, silicon-nitride (Si_3N_4) AFM cantilever probes with integrated pyramid tips (model no. MLCT-AUHW, Veeco Metrology Group, Santa Barbara, CA) (*see* **Notes 3** and **4**).
9. Silicone-bottom plastic containers for storing and organizing individual AFM probes (e.g., TipBox®; BioForce Nanosciences, Ames, IA) (*see* **Fig. 4C**).
10. Ultrasharp® silicon calibration grating with a regular pattern of sharp points having a cone angle <10° and tip radius <10 nm (cat. no. TGT01, Silicon-MDT, Moscow, Russia, available from K-TEK International, Portland, OR) for characterizing the shape, angle, and radius of curvature of AFM probe tips.
11. Micromachined silicon force calibration cantilevers (model no. CLFC-NOBO, Veeco Metrology) for calibrating the AFM probe spring constant.
12. Optional ozone/UV (ultraviolet) decontamination chamber (e.g., Ozone PSD-II; Novascan Technologies, Ames, IA) for cleaning and reusing expensive custom AFM probes.

2.3. AFM System

1. Atomic force microscope compatible with operation in fluid (*see* **Note 1**), including controller electronics and driver software.
2. Inverted light microscope (model IX-70, Olympus) with 10×, 20×, and 40× long working distance objective lenses and trinocular head adapter for video camera mount (*see* **Note 5**). The microscope stage is typically a custom part designed to support a particular model of AFM and supplied by the AFM manufacturer. The stage itself should be adjustable to facilitate alignment of the AFM probe over the objective lens and should also allow separate *x*-*y* translation of the sample relative to the AFM probe.

3. A gooseneck fiberoptic light source (Fiber-Lite 190; Dolan-Jenner, Lawrence, MA) provides illumination of the sample by shining light into the AFM head, which has a built-in mirror for directing the light downward toward the objective lens on the inverted microscope. Manual adjustment of the fiberoptic lamp position can dramatically alter shadowing and contrast for visualizing the cell culture sample.
4. Bioscope fluid sample heater (Digital Instruments) for maintaining cells at a physiological temperature of 37°C. To minimize evaporation of fluid and resulting changes in osmolarity of the cell culture medium and to avoid condensation of fluid on the inner electronics of the AFM scanner, this heater is supplied with special silicone covers that fit over a standard 60-mm culture dish during AFM scanning (*see* **Note 6**).
5. A vibration isolation platform (e.g., Stable Table; VayTek, Fairfield, IA) to minimize vertical and horizontal mechanical vibration of the microscope. Placing the AFM on a slab of solid marble and suspending it from the ceiling using bungee cords can be an effective alternative ***(4)***.
6. A video camera mounted on the trinocular head of the microscope and connected to a screen and VCR provides a convenient means of visualizing and recording AFM experiments and monitoring the condition and stability of the cell culture. For low-light fluorescence applications, we use a cooled digital video camera (Sensicam, Cooke Corp, Auburn Hills, MI) with an optional remote fan to minimize mechanical vibration on the microscope. The camera is connected to the microscope using a 0.63× coupler lens (model no. D63IXC; Diagnostic Instruments, Sterling Heights, MI) so that the magnification and field of view in the camera match that in the oculars.

3. Methods

Before beginning these procedures, the AFM controller, video monitors and computers, vacuum pump, lamps, and other major electronics should be turned on and warmed up for at least 60–90 min to achieve a stable temperature and to minimize drift of electrical signals during the experiment.

3.1. Preparing and Mounting the AFM Probe

The following methods for preparing and mounting the AFM cantilever probe on the scanner head will help minimize damage to the cells, the probes, and the scanner.

1. Carefully separate a row of rectangular chips from the wafer of cantilevers (*see* **Fig. 4**) by lifting one end, then the other, with a pair of broad-tipped microscopic tweezers. Holding the row of chips with one pair of tweezers, use a second pair to separate individual chips by carefully snapping them apart at the score line. Arrange the individual chips in a TipBox® for subsequent use.
2. Using microscopic tweezers, carefully grasp one chip from the side and examine under the dissecting microscope to inspect for bent, broken, or dirty probes. Stabilizing the chip against the dissecting scope stage with tweezers, use a 30G needle in the other hand to carefully break off any probes longer than the one selected

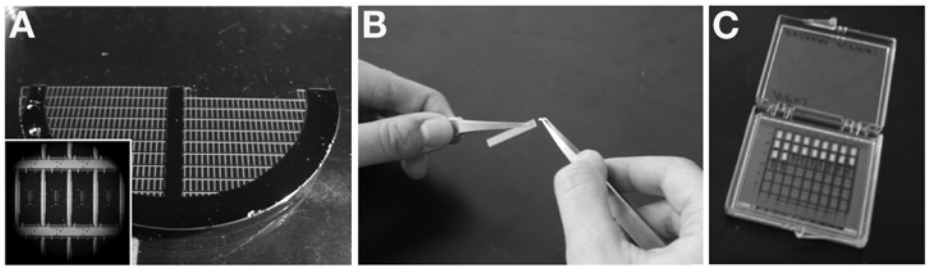

Fig. 4. **(A)** A half-wafer of Microlever probes with one row that has been removed. Inset shows magnified view of a region of the wafer. **(B)** Individual chips must be snapped off the end of a connected row. **(C)** Separated chips are arranged in a silicone-bottom storage box.

for the experiment (*see* **Note 3**). Only this one probe will be monitored by the AFM laser, and longer probes could contact and potentially damage the cell undetected.

3. Carefully mount the chip on a holder appropriate for use in fluids and inspect once more to ensure that the probe is undamaged.
4. Mount the holder on the AFM scanner and then hold the scanner over a Kimwipe® at about a 20° angle with the probe facing down. Using a 30G needle on a 3-mL syringe, carefully apply a few drops of culture medium alongside the AFM probe, allowing fluid to engulf the probe without introducing air bubbles and without dripping down into the scanner (*see* **Note 7**).
5. Right the scanner, move it onto the inverted microscope stage, and plug it in; then use the stepper motor to lower it into a small volume of culture medium on a glass slide (or mica sheet). Use just enough fluid (approx 2 mL) to form a meniscus between the probe holder and the glass slide. Adjust the fiberoptic light and focus to view the AFM probe using the inverted microscope. If any air bubbles are observed, remove the scanner, remove the probe holder and carefully blot it dry with the corner of a Kimwipe® or cotton swab and compressed air; repeat **step 4**.
6. Adjust the laser spot so that it reflects off the tip of the cantilever (the optical microscope is very helpful for this step) and provides an adequate voltage signal centered on the photodetector. The photodetector voltage should be monitored for several minutes to ensure that the system has stabilized, as the probe might deflect as it is heated by the laser.
7. Use the stepper motor to carefully move the AFM toward the glass slide (*see* **Note 8**). Adjust the set-point reference voltage to 0 V, the vertical deflection voltage to about –1 V, and the horizontal deflection voltage to 0 V. Also set the scan size to zero so that the probe remains stationary when it initially contacts the glass surface (and later the cell). Finally, use the AFM control software to automatically advance the probe until it makes contact, or engages, on the glass slide with a force proportional to the difference between the vertical deflection voltage and the set-point reference voltage.
8. In contact force mode, perform an indentation test on the glass slide. The *z*-range and scan rate can be adjusted by the user and should be set to values comparable

to what will be used with the cell indentation experiments. We have found that typical values of 3 μm for *z*-range and 1 Hz for scan rate work well for many cell types. Note that because the slide is effectively rigid compared to the stiffness of the cantilever, there is no indentation, so for every nanometer that the probe advances, the tip deflection should increase by exactly 1 nm. The resulting measurements of tip deflection vs probe position (the "force curve") should ideally have a flat precontact region with an abrupt transition to a linear postcontact region (*see* **Fig. 1B**).

9. A manual trace of the linear postcontact curve provides a conversion factor, or detector sensitivity, in nanometers per volt that is used to convert the photodetector signal into probe deflection.

For standard AFM imaging applications, the shape of the precontact region of the force curve is of little consequence. However, for cell indentation studies, the transition from precontact to postcontact is often subtle and gradual. Determination of this contact point is most accurate and reliable when the precontact portion of the curve is ideally flat and linear with minimal noise. We, therefore, make an extra effort to optimize the shape of the precontact region as follows:

1. Withdraw the AFM probe approx 1 mm from the glass slide. Readjust the set point and horizontal deflection voltages to 0 V, and set the vertical deflection voltage to about +1 V; then engage the AFM tip. Setting the vertical deflection above the set point will cause the AFM controller software to think the tip is immediately in contact with the sample even though it is not (note that the control-F key sequence can also be used with Digital Instruments Nanoscope software to perform such a "false engage").
2. In the contact force mode, perform a series of repeated excursions of the AFM probe over the full *z*-range of the scanner. Because the probe is far from any surface, the resulting force curve should ideally be a straight flat line indicating zero probe deflection. We have found that by adjusting the location of the laser spot on the AFM probe, it is possible to drastically alter the shape of this noncontact curve: The curve can be nonlinear and can exhibit oscillatory reflection artifacts, and the overall slope can switch from positive to negative (*see* **Fig. 5**). We typically aim for a force curve in which the deviation from a flat straight line is less than 4 nm over the full *z*-range of the scanner, at times accepting some nonlinearity to obtain the maximum possible smoothness.
3. Once the laser position has been optimized, it should not be adjusted for the remainder of the experiment. Withdraw the AFM probe and repeat **steps 7–9** above to determine the sensitivity of the photodetector with the laser in its new optimized location on the probe. If the laser position is accidentally altered during an experiment, this process should be repeated before force measurements are resumed.
4. Withdraw the AFM probe several millimeters using the stepper motor, and then lift the scanner to ensure that nothing bumps the probe when the glass slide is removed and exchanged for another sample.

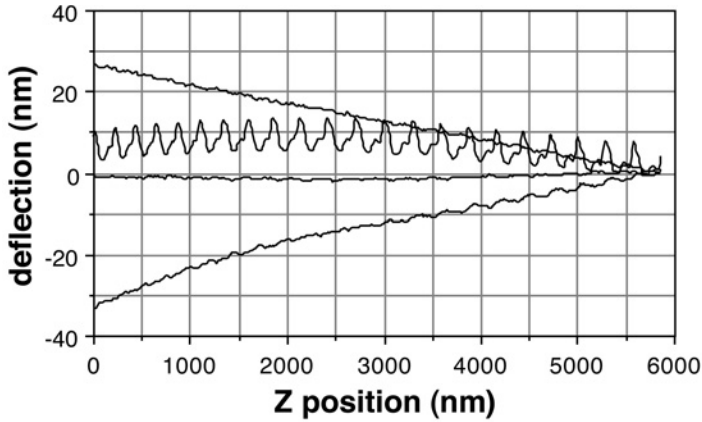

Fig. 5. Four examples of noncontact force curves in water (retraction data omitted for clarity) obtained using a single cantilever undergoing repeated 6-μm excursions at 1 Hz. By altering the position of the laser reflection near the end of the cantilever, substantial deviations from the ideal zero-deflection noncontact curve could be observed.

3.2. AFM Probe Characterization

The two main characteristics of the AFM cantilever probe that must be accurately determined for each experiment are (1) the spring constant, κ, which is required to compute contact force from probe deflection, and (2) the tip geometry, which is required to accurately extract the elastic modulus from the force–depth indentation response. Although nominal values of spring constant and tip radius might be adequate for some purposes such as mapping of relative stiffness on a single cell, accurate evaluation of cell mechanical properties and comparison from one experiment to another requires more careful probe characterization.

3.2.1. Spring Constant

The spring constant of the AFM probe is required to compute the contact force from the measured probe deflection (*see* **Note 9**). Several alternative methods have been proposed for experimentally determining the spring constant of an AFM cantilever from measurements of its resonance frequency *(40–42)* or thermal noise behavior *(29)*. We prefer another simple method using a reference cantilever for calibration *(43,44)*. This method requires no assumptions about the geometry of the AFM probe, it can be performed in an aqueous environment, and the probe undergoes a bending mode of deformation consistent with cell indentation experiments. The calibration process is as follows:

1. Carefully mount a calibration cantilever on a clean dry glass slide using a small piece of double-stick tape.
2. Add a few drops of deionized water alongside the probe using a 3-mL syringe with a 30G needle, again using caution to avoid introducing air bubbles as the liquid

engulfs the chip. Place this slide on the microscope stage and lower the AFM scanner until a meniscus forms between the AFM probe and the calibration cantilever, carefully adding drops of liquid with the syringe as needed (*see* **Note 10**).

3. Engage the AFM tip on the glass as described in **step 7** of **Subheading 3.1.** for determining the photodetector sensitivity.
4. Obtain a force curve on the glass slide as described in **step 8** of **Subheading 3.1.** and save this measurement in a data file.
5. Withdraw the scanner several millimeters using the stepper motor.
6. Engage the AFM tip on the end of the calibration cantilever (*see* **Note 11**).
7. Obtain a force curve on the calibration cantilever using the same scan settings as in **step 4** and save this measurement in a data file. In this case, the force curve should also have a linear postcontact region, but the slope should appear less than on glass because of bending of the calibration cantilever by the AFM probe.
8. Withdraw the AFM probe several millimeters using the stepper motor and then lift the scanner to ensure that nothing bumps the probe when the calibration cantilever is removed and exchanged for another sample.
9. Export the two above data files and fit a straight line to the postcontact data to obtain the slope of this region. The slope on glass, m_g, should ideally be unity (i.e., 1000 nm/μm). The slope on the calibration cantilever, m_c, should have a smaller value. From these two values and the known spring constant of the calibration cantilever, κ_c, one can compute the spring constant of the AFM probe, κ_p, using the formula $\kappa_p = \kappa_c(m_g - m_c)/(m_c \cos\theta)$, where θ is the acute angle between the AFM probe and the calibration cantilever (typically about 10°, depending on how the probe is mounted on the particular model of AFM scanner).

3.2.2. Tip Geometry

As will be described in **Subheading 3.5.2.**, quantification of cell mechanical properties from AFM indentation measurements requires accurate knowledge of the geometry of the AFM probe tip (*see* **Note 12**). To characterize tip geometry, one can use scanning electron microscopy to obtain a high-resolution image of the tip (*see* **Fig. 2D**). However, this requires special facilities and is often inconvenient and costly to perform on a regular basis. A simple alternative is tip self-imaging ***(45)***, in which the AFM probe is scanned over a sample with very sharp features compared to the tip geometry, yielding a reversed image of the tip itself (*see* **Fig. 6**).

1. Carefully mount the Ultrasharp® silicon calibration grating on a clean dry glass slide using a small piece of double-stick tape. Then add fluid and transfer to the AFM stage as described in **step 2** of **Subheading 3.2.1.**
2. Engage the AFM tip on the calibration grating using the procedure described in **step 7** of **Subheading 3.1.**, using caution to not crash the probe and damage the calibration grating.
3. In the contact imaging mode, increase the *x*-*y* scan size to about 5 μm, using a scan speed of about 1 Hz and a low pixel resolution (128 pixels) to get a quick image of the tip. Use the *x*-axis and *y*-axis offset controls to center the probe tip in the

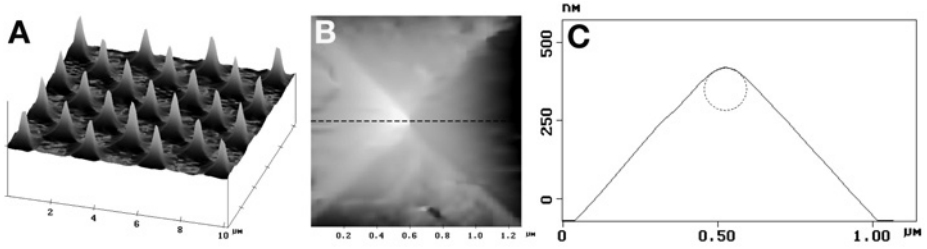

Fig. 6. **(A)** 10 × 10-µm contact mode scan of an Ultrasharp® calibration grid with expanded *z* scale. **(B)** Magnified 1.27-µm scan of a single sharp feature (top view) reveals a reverse image of the pyramidal Si_3N_4 AFM probe tip. **(C)** A 1:1 aspect ratio cross-section through the peak of the height image (broken line in B) reveals a blunt tip with a 70-nm radius of curvature indicated by the dotted circle.

image and adjust the scan size as needed to capture the tip geometry. Then perform a final scan at high pixel resolution and save this image file.

4. The file can then be exported and analyzed using image processing software to determine the radius of curvature of the probe tip (*see* **Fig. 6C**), or the AFM software might have this capability built in it.

3.3. Cell Indentation

3.3.1. Cell Culture Preparation

Analysis of mechanical properties by AFM indentation is compatible with standard cell culture techniques for most adherent cell types using confluent or subconfluent monolayer cultures in a small (e.g., 60 mm) culture dish or similar flat, stiff substrate (*see* **Note 13**). Prior to moving the cells onto the stage of the AFM, standard cell culture medium should be removed and replaced with a minimal volume (e.g., 2–3 mL in a 60-mm dish) of CO_2-independent medium (*see* **Notes 2** and **7**) and the cells should be allowed to equilibrate to the temperature at which the AFM experiment will be conducted.

3.3.2. Single-Force Curves

The most fundamental cell mechanics experiment performed using the AFM is the simple indentation test described as follows:

1. After placing the cell culture dish on the microscope stage, use the stepper motor to lower the AFM until it makes contact with the surface of the cell culture medium. Center the laser reflection on the photodetector and monitor its position for several minutes, as it will tend to drift until the probe and sample become thermally equilibrated.
2. Adjust the set-point reference voltage to 0 V, the vertical deflection voltage to about –1 V, and the horizontal deflection voltage to 0 V. Also set the *x*-axis and *y*-axis

offsets to zero and the scan size to zero so that the probe remains stationary when it initially contacts the cell. Finally, align the probe tip with a region of interest as described in **Note 11** and use the AFM control software to automatically advance the probe until it engages on the cell at the desired location.

3. In the contact force mode, perform an indentation test on the cell. The *z*-range and scan rate should be adjusted by the user to obtain a desirable force curve. We have found typical values of 3 μm for *z*-range and 1 Hz for scan rate to work well for many cell types. The ideal force curve should have a flat precontact region that transitions around one-half to three-quarters of the way through the *z*-excursion to a nonlinear postcontact region where the AFM tip is indenting the soft cell (*see* **Fig. 1B**). Hysteresis between the advancing and retracting portions of the curve might also be observed (*see* **Notes 14** and **15**).
4. Save these measurements of tip deflection vs probe position in a data file. Performing multiple indentations at the same location is one way to evaluate stability of the cells to characterize potential changes in cell properties in response to probing.

3.3.3. Arrays of Force Curves (Force Mapping)

Considering the highly localized nature of AFM indentation measurements obtained using a standard probe and the substantial regional variability of the cytoskeleton and other intracellular structures, single-indentation tests might be inadequate to characterize cell mechanical properties for some applications. Another approach is to perform an array of indentations covering some region of interest on the cell, which then allows evaluation of the variability in the measurement and also can be used to map the elastic properties of the cell ***(13,46)***. This can be combined with contact mode imaging (and fluorescence microscopy) to correlate elastic properties with specific cytoskeletal structures.

1. A simple assessment of regional variability of cell mechanical properties can be obtained by performing several indentations in a small array in the region of interest. A square array of up to 4×4 indentations covering up to a 5×5-μm region of the cell provides a relatively rapid (<30 s) assessment of local mechanical heterogeneity, with the variability tending to decrease as the size of the region probed also decreases. This is easiest when the AFM controller software allows such indentation arrays to be executed automatically, although such an experiment could also be performed by adjusting the *x*-axis and *y*-axis offsets manually.
2. Cell indentation can also be used to obtain a more detailed map of mechanical properties. Such "force mapping" techniques generally involve performing a much larger array of indentations (16×16 to 128×128 locations) covering a substantial region (up to 100×100 μm) of one or more cells (*see* **Note 16**). The actual indentation force, or some derived measure of elastic properties, is then rendered at each location to form an image with each pixel representing one of the indentation sites (see **Subheading 3.6.** for further details). Note that the acquisition time for such arrays of force curves can be quite long (hours), during which time it is

important to maintain a stable culture environment and have some independent verification of cell viability (such as video microscopy).

3. To obtain structurally correlated information on mechanical properties with more rapid scan times, it is possible to combine indentation arrays with contact mode imaging (*see* **Note 17**). With the AFM probe withdrawn a few hundred microns above the cell, adjust the set-point reference and the horizontal deflection voltages to 0 V and the vertical deflection voltage to about –0.5 V to engage at a relatively low contact force. Also set the scan size and *x*- and *y*-axis offsets to zero. Engage the AFM tip at the desired location on the cell (*see* **Note 11**). Set the *x*-*y* scan speed to 1 Hz or less and increase the scan size to obtain a contact mode image of the desired region of interest (*see* **Note 18**). Based on this image, use the mouse to graphically zoom in on a region of the cell with features of interest. With the new scan size and *x*-axis and *y*-axis offsets so determined, switch to the force mapping mode to obtain an array of indentations as described in **step 2.**

3.4. Cleaning Up

1. At the end of the experiment, withdraw the AFM probe and use the stepper motor to back up the scanner nearly to the limit of the focus range of the optical microscope. This keeps the scanner distant enough to avoid damage when exchanging samples, yet close enough to use the optical microscope to view the AFM probe during setup for the next experiment (*see* **Subheading 3.1.**).
2. Unplug the scanner and remove the probe holder. Use microscopic tweezers to remove the probe and set it aside. Rinse the holder thoroughly with deionized water, dry with the corner of a Kimwipe® or cotton swab, and blow dry with the compressed air duster. Alcohol and other solvents can be used for cleaning calibration standards, but they should not be used on the AFM probe holder to avoid damaging delicate parts.
3. The probe can be disposed of or be rinsed and saved for ozone/UV cleaning and reuse. Note that ozone cleaning can erode and alter the AFM tip, so the tip geometry of reused probes should be characterized as in **Subheading 3.2.2.**

3.5. Data Analysis

The most prevalent method of analyzing AFM indentation data has been application of the so-called "Hertz model" of contact between a rigid indenter and an elastic sample *(47,48)*. However, it is important to appreciate that the Hertz model makes a number of simplifying assumptions that do not readily apply to the cell indentation problem; these include infinitesimal deformation of a semi-infinitely thick and flat sample, having homogeneous isotropic linear elastic material properties, and using an axisymmetric indenter *(37,49)*. We have developed a more generalized analysis method whereby computation of an apparent elastic modulus as a function of indentation depth can reveal when deviations from the standard Hertz model become important *(37)* (*see* **Note 19**).

The two main steps in the analysis are identifying the initial point of contact with the cell and calculating the pointwise elastic modulus.

3.5.1. Identifying the Contact Point

When indenting a stiff sample, the contact point is readily apparent as an abrupt transition from the precontact region to the postcontact region, as described in **step 8** of **Subheading 3.1.** However, when indenting a cell, the initial contact event occurs when the smallest part of the tip contacts the soft cell membrane, resulting in a smooth and continuous transition from the precontact to postcontact region, as described in **step 3** of **Subheading 3.3.2.** Accurately identifying the initial point of contact, which impacts most subsequent analyses of cell mechanical properties, is not a trivial matter. A number of procedures have been proposed to identify the contact point by fitting some portion of the postcontact data to the Hertz model ***(27,50,51)***. However, when the data deviate from the expected theory, the estimated contact point can become clearly inaccurate ***(35)***. We have therefore developed a two-part polynomial model-fitting algorithm that utilizes both precontact and postcontact data to identify the contact point (*see* **Fig. 7**). This iterative fitting procedure takes just a few seconds per force curve when implemented in Matlab on a personal computer.

1. Using the advance portion of the force curve, select a subset of the data clearly in the precontact region and calculate the average precontact deflection. Also, the z-position data are negated so that the postcontact regime has a positive slope (i.e., increases to the right, rather than to the left, as it is acquired in the standard force curve).
2. Specify a maximum deflection that will be included in the postcontact fit, capturing the earliest portion of the indentation response. A value of 15 or 20 nm beyond the precontact deflection is typical. Begin by assuming a trial contact point, z^{trial}, that corresponds to the data point at half this maximum deflection.
3. Use a standard Levenberg–Marquardt least squares minimization algorithm ***(52)*** to fit the following two-part polynomial model of probe deflection to the data in the specified neighborhood of the trial contact point, z^{trial},

$$h(z) = \begin{cases} a_1 + b_1 z & \text{for } z \le z^{\text{trial}} \\ a_2 + b_2 (z - z^{\text{trial}}) + c_2 (z - z^{\text{trial}})^2 & \text{for } z > z^{\text{trial}} \end{cases}$$

   where a_1, b_1, b_2, and c_2 are model parameters adjusted in the fitting procedure, and the constraint $a_2 = a_1 + b_1 z^{\text{trail}}$ is enforced to ensure continuity between the precontact and postcontact regimes.
4. Record the resulting value of the minimization error function for this value of z^{trial}.
5. Moving one data point at a time toward the beginning of the precontact region, repeat **steps 3** and **4** using each data point sequentially as the trial contact point for the fitting procedure (*see* **Fig. 7A**).

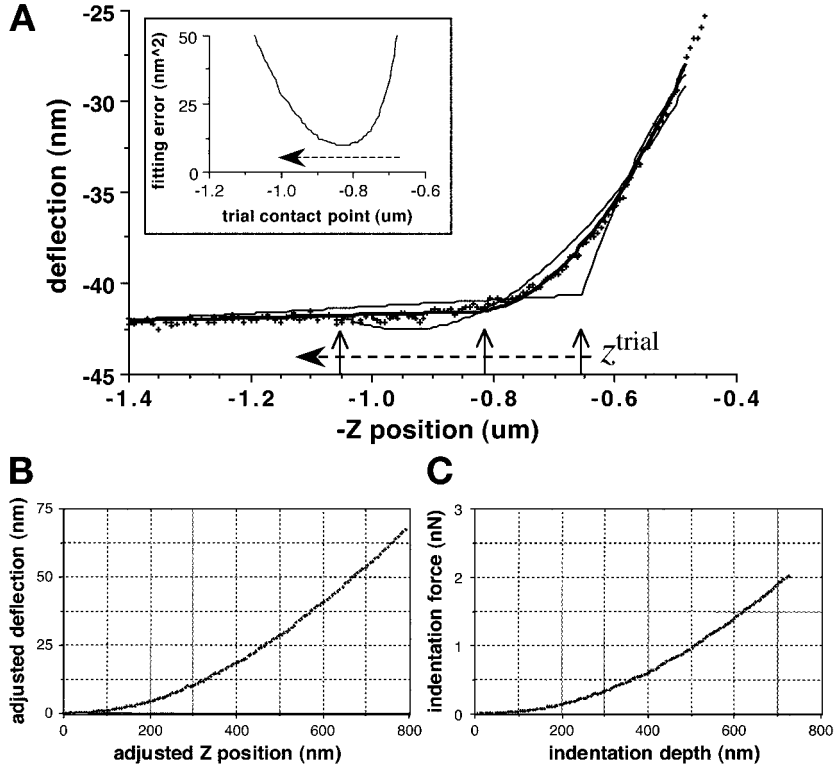

Fig. 7. Analysis of indentation data obtained from the advance portion of the force curve in **Fig. 1B**. **(A)** Procedure for identifying the contact point using a two-part polynomial model-fitting algorithm (*see* text for details). The data scale is expanded to highlight the region of initial contact. Inset shows the fitting error function vs the trial contact point, the minimum of which is used to determine the actual contact point. **(B)** The adjusted postcontact deflection vs z-position with the origin at the contact point. **(C)** The resulting indentation force-vs-depth curve.

6. A plot of the minimization error vs z^{trial} will exhibit a minimum value for the data point at which a best fit is obtained between the linear precontact region and the quadratic (or other polynomial) initial postcontact region (*see* **Fig. 7A,** inset). This data point provides an estimate of the contact point.
7. Finally, the fitting routine is repeated one last time, with the contact point itself included as a fitted model parameter in case the actual point of contact, z^*, occurred somewhere in between two acquired data points.
8. Subtract the (z^*, h^*) coordinates of the contact point from the (z, h) values of each data point, i, in the force curve so that the contact point is shifted to become the origin of the curve using $(z', h')_i = (z, h)_i - (z^*, h^*)$. Precontact data are discarded, leaving the postcontact data (*see* **Fig. 7B**).

9. For each data point, the cantilever spring constant is used to calculate the indentation force, $F = \kappa \times h'$. With κ in newtons/meter (N/m) and h' in nanometers (nm), F has units of nanonewtons (nN). The indentation depth (nm) is calculated using $D = z' - h'$. The resulting plot of indentation force vs depth (*see* **Fig. 7C**) is used to determine the elastic modulus of the cell.

3.5.2. Calculating the Pointwise Modulus

In theory, the indentation force and depth are related by an equation of the form *(37)* $F = 2\pi \times \tilde{E} \times \phi(D)$, where $\tilde{E}$ is an apparent elastic modulus that is equivalent to $E/2(1-\nu^2)$ in classical linear elasticity theory, with E being the Young's modulus and $\nu = 0.5$ being the Poisson's ratio for an incompressible material. The term $\phi(D)$ is an expression determined by the geometry of the AFM probe tip. For a blunt-tipped cone with tip angle, 2α, that transitions at radius b into a spherical tip of radius R, the geometric term is determined as follows *(37,53)*.

For indentations smaller than the tip defect ($D < b^2/R$), the equation is that for a simple spherical indenter:

$$\phi(D) = \frac{4}{3\pi}\sqrt{RD^3}$$

For indentations larger than the tip defect ($D \geq b^2/R$),

$$\phi(D) = \frac{2}{\pi}\left\{aD - \frac{a^2}{2\tan\alpha}\left[\frac{\pi}{2} - \arcsin\left(\frac{b}{a}\right)\right] - \frac{a^3}{3R} + \sqrt{a^2-b^2}\left[\frac{b}{2\tan\alpha} + \frac{a^2-b^2}{3R}\right]\right\}$$

where the radius of contact, a, is determined from the following expression:

$$D - \frac{a}{R}\left(a - \sqrt{a^2-b^2}\right) - \frac{a}{\tan\alpha}\left[\frac{\pi}{2} - \arcsin\left(\frac{b}{a}\right)\right] = 0$$

A smooth transition from the cone to the spherical tip is obtained when $b = R\cos\alpha$ The indentation response for a standard pyramidal silicon nitride probe is equivalent to that for a cone with $\alpha = 39.5°$ *(37)*; a tip defect with R in the range 50–100 nm is typical (*see* **Subheading 3.2.2.**).

In the general equation $F = 2\pi \times \tilde{E} \times \phi(D)$, the indentation force and depth are measured in the AFM experiment and $\phi(D)$ is determined from the tip geometry as above (*see* **Note 20**). Therefore, the only unknown is $\tilde{E}$. Rather

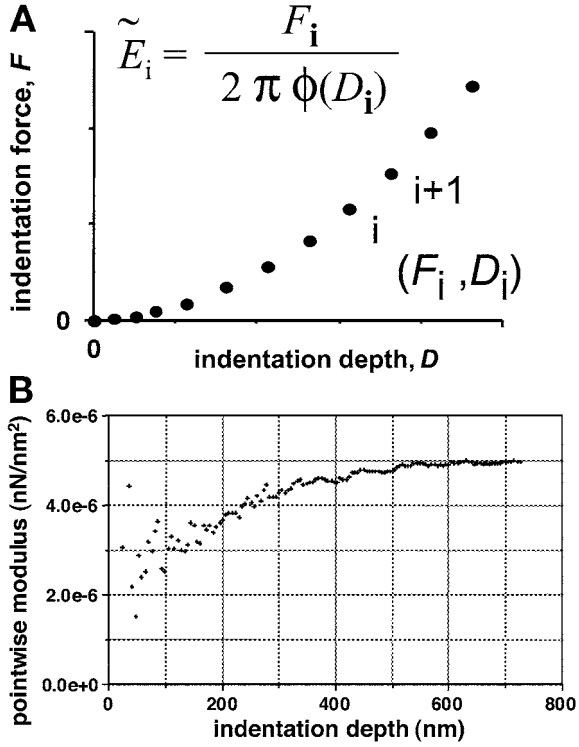

Fig. 8. **(A)** Schematic procedure for calculating the pointwise elastic modulus $\tilde{E}_i$, from individual indentation force–depth data points. **(B)** Plot of pointwise modulus vs indentation depth obtained from data in Fig. 7C.

than assume that $\tilde{E}$ is constant *a priori* (*see* **Note 21**), we solve the equation at each data point, *i*, to obtain a pointwise apparent modulus, $\tilde{E}_i = F_i/(2\pi\phi(D_i))$, as illustrated in **Fig. 8**. With *F* in n*N* and *D* in nm, $\tilde{E}$ has units of nN/nm^2, where 10^{-6} nN/nm^2 = 1000 N/m^2 = 1 kPa.

The elastic properties of the cell are determined from a plot of the pointwise modulus vs indentation depth *(37)*. Changes in the value of $\tilde{E}_i$ indicate deviations from the classical linear elastic Hertz model.

3.6. Data Presentation

The above pointwise modulus analysis can reveal details of local cell mechanical properties that are simply ignored in more traditional analysis methods. However, the increased complexity of the resulting data impacts its subsequent presentation and interpretation. We have found the following

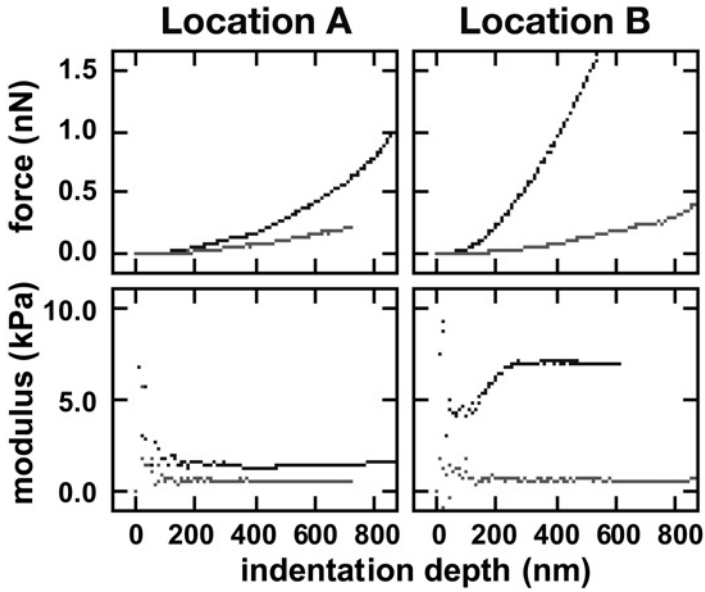

Fig. 9. Indentation force and corresponding pointwise modulus vs indentation depth at two locations 2 μm apart on a living NIH 3T3 fibroblast cell. The two curves in each panel were obtained under control conditions (upper curve) and after 30 min treatment with cytochalasin-B (lower curve).

methods useful for conveying regional variations in the pointwise modulus and correlating these with local cytoskeletal structures.

3.6.1. Pointwise Modulus Curves

A plot of pointwise modulus vs indentation depth directly reveals how the apparent stiffness of the cell varies as it is deformed. For example, measurements on a control NIH 3T3 fibroblast cell (*see* **Fig. 9**) show that $\tilde{E}_i$ can be nearly constant with indentation depth at one location, whereas it can exhibit a strongly increasing depth dependence at a neighboring location just 2 μm away. The increased apparent stiffness with depth might reflect nonlinear elastic properties (sometimes incorrectly called "strain hardening") typical of macroscopic biological tissues or it might reveal through-thickness heterogeneity of material properties, with the AFM interacting with stiffer structures as it probes deeper into the cell. AFM indentation of the same cell following treatment with cytochalasin-B (4 μM for 30 min) results in smaller values of $\tilde{E}_i$ that are essentially independent of indentation depth or location on the cell, suggesting that the previous nonlinear behavior could have been primarily the result of the filamentous actin cytoskeleton, and not simply an artifact of the underlying stiff substrate.

Because the value of $\tilde{E}_i$ can vary substantially with indentation depth, it is necessary to specify the indentation depth when comparing modulus values. Linear interpolation between nearest-neighbor data points can be used to easily obtain modulus values at specific indentation depths for performing descriptive and comparative statistics.

3.6.2. Arrays of Modulus Curves

By performing a more detailed force mapping of a region of a cell, it is possible to correlate the mechanical behavior with underlying cytoskeletal structures. **Figure 10A** shows a contact mode AFM image of a 15 × 15-μm square region of the periphery of a human aortic endothelial cell cultured on a polystyrene dish at room temperature, showing linear structures representing actin stress fibers within the cell. The black square indicates a 3.5 × 3.5-μm subregion where the AFM was zoomed in on an area of interest with a prominent diagonal stress fiber. An 8 × 8 array of 64 indentations was performed in this subregion at an indentation rate of 3 μm/s, and the resulting pointwise modulus curves are plotted in a matrix corresponding to their relative location on the cell (*see* **Fig. 10B**). Strongly nonlinear behavior is exhibited in a diagonal zone coincident with the prominent stress fiber, whereas adjacent regions appear softer with less depth variation.

3.6.3. Images of Regional Stiffness

Arrays of modulus curves as described above contain a tremendous amount of information about the detailed regional and depth-dependent mechanical properties of living cells. However, presented as such, the data can be overwhelming and not ideally suited for presentation in a figure or to an audience. One alternative is to extract the pointwise modulus at a specified indentation depth and create an image in which this modulus value is represented on a gray scale, (i.e., image contrast is based on the local cell stiffness). The resulting image of elastic properties (an "elastogram" ***[13]***) provides a convenient visual representation of the regional cell stiffness, although it must be emphasized that with nonlinear elastic behavior, the appearance of the map can vary substantially at different indentation depths. **Figure 10C** shows an example of such an elastogram, with $\tilde{E}_i$ extracted at $D = 200$ nm for the same region represented by the array of modulus curves described earlier. This representation makes it clear that the actin stress fibers are stiffer than the surrounding cytoplasm. However, only by examining the individual modulus curves can one also appreciate that the stress fibers selectively give rise to nonlinear elastic properties, whereas the cytoplasm behaves like a nearly linear elastic material.

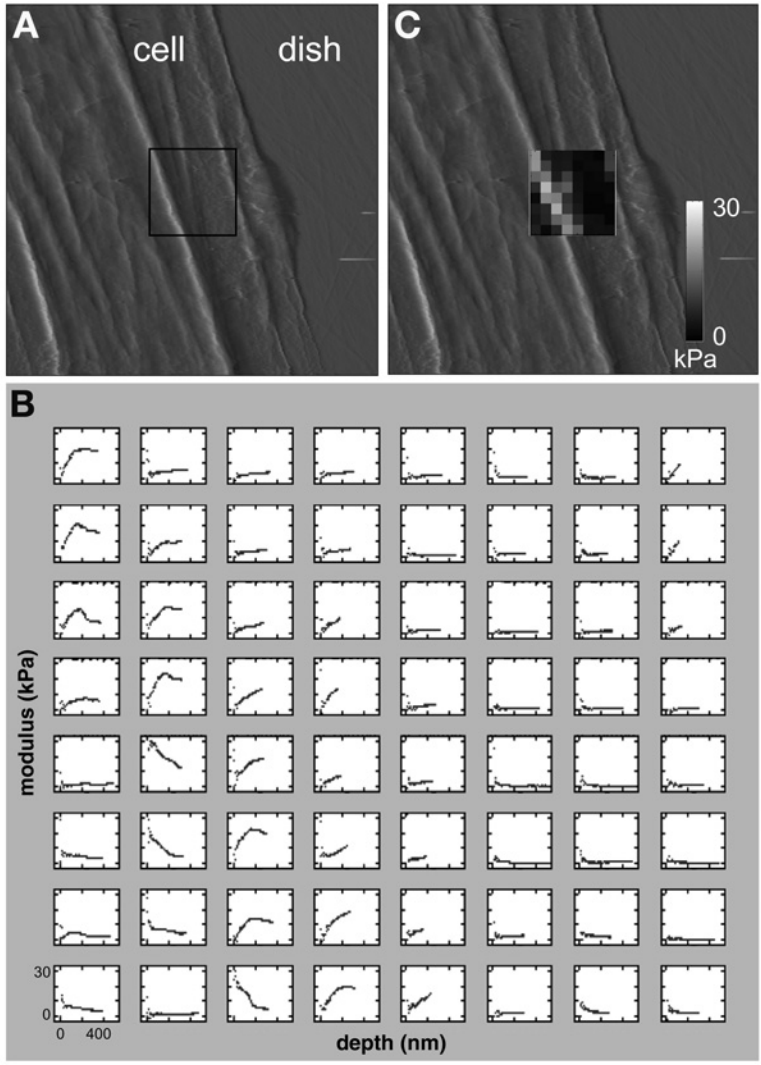

Fig. 10. **(A)** Contact mode AFM image (15 × 15 μm) of the peripheral region of a human aortic endothelial cell, revealing cytoskeletal actin stress fibers. The black square indicates a 3.5 × 3.5-μm region where an 8 × 8 array of 64 indentations was performed to measure local cell mechanical properties. **(B)** Pointwise modulus vs indentation depth from the 8 × 8 array of indentations described in **A**. All curves are shown on the same scale of 0–30 kPa for modulus and 0–400 nm for depth. **(C)** The same contact mode image as **A**, with a superposed gray-scale map of the pointwise modulus from **B** extracted at 200 nm depth.

4. Notes

1. Most commercial AFMs are supported on a three-point frame, with the instrument placed on top of the sample. Alternatively, the Bioscope (Digital Instruments, Santa Barbara, CA) is supported from behind such that the end of the scanner (where the AFM probe is mounted) remains exposed. This permits easy access to the sample and direct visualization of the probe and the fluid volume. It also facilitates compatibility with fluid-exchange systems, electrical stimulators, micropipet manipulators, and other techniques and devices useful for cell biology experiments.
2. When used according to the manufacturer's instructions, this special CO_2 independent culture medium allows cells to be maintained in a normal room-air environment for several hours while maintaining a constant pH, unlike normal bicarbonate-buffered culture media. Naturally, if the AFM is equipped with an environmental chamber that maintains a physiologic 5 to 10% CO_2 environment, this special media is not necessary.
3. A broad range of AFM cantilevers are commercially available, offering variations in shape, stiffness, material composition, surface coating, and tip geometry to satisfy a wide range of AFM applications. Here, we recommend unsharpened, gold-coated, silicon nitride Microlevers® (*see* **Fig. 2**), which are well suited for cell indentation studies for a number of reasons. Unsharpened pyramidal probe tips minimize cell damage and help maintain viability for extended scans ***(4,54,55)***. Sharpened tips offer higher resolution for some AFM imaging applications but tend to penetrate the cell membrane and damage living cells ***(56)***. Gold coating enhances reflectivity for use with cell culture media containing phenol red, which attenuates AFM laser light. Silicon nitride (Si_3N_4) Microlevers® are fabricated with six cantilevers per chip, having spring constants ranging from 0.01 to 0.5 N/m. It is important that the spring constant of the probe be well matched to the sample stiffness. If the probe is too stiff, it will not deflect during contact and could damage the cell; if the probe is too soft, it will not indent the cell sufficiently to obtain reliable material properties. Typically, a spring constant of 0.02–0.1 N/m works well with most biological cells.
4. Commercial AFM probes are microfabricated in wafers of several hundred at a time ***(57,58)***. Whereas stoichiometry, thickness, and tip characteristics can vary from one wafer to another, AFM probes from a single wafer are often quite consistent ***(40,59,60)***. Therefore, it is advisable to purchase AFM probes in wafers or half-wafers to maximize consistency and minimize cost to less than $10 per probe, making it practical to use a new probe for each experiment.
5. If the inverted microscope is to be used exclusively with the AFM, then the standard microscope lamp and condenser components are not required because the AFM blocks this light path. The AFM is also compatible with (standard or confocal) fluorescence microscopy ***(30,61)***, offering a powerful tool for mechanotransduction studies relating specific molecular responses to targeted force simtuli. As such, the light microscope and video monitoring system are very useful but not absolutely necessary. Some investigators have used a standard AFM configuration without a light microscope to probe confluent monolayer cell cultures without

direct visualization *(28)*, although this approach is obviously limited for targeting and monitoring individual cells.

6. Various custom enclosures and heating systems have been built for the purpose of maintaining cells at body temperature *(4)*, including placing the entire AFM in a warm room *(28)*. Such systems must be very stable to minimize thermal fluctuations of the cantilever. The advantage is a more physiologic environment during the experiment. Alternatively, performing experiments at room temperature could slow metabolic processes and make the cells more stable during lengthy protocols.
7. Dangerously high voltages are required to drive the piezoelectric elements controlling the probe position. It is especially critical when working in saline solutions that no liquid comes in contact with the scanner electronics, as this could severely damage the instrument. The scanner should be regularly inspected, cleaned, and calibrated according to the manufacturer's instructions to ensure that it is operating properly. If any fluid leakage is suspected during an experiment, unplug the scanner immediately and dry off all components with compressed air and cotton swabs, inspecting it under the dissecting microscope.
8. Adjusting the laser spot and making gross adjustments of the scanner position relative to a transparent sample are both greatly simplified when the AFM is mounted on an inverted light microscope for direct visualization. To avoid accidentally crashing the AFM tip into the clean transparent glass slide, it is helpful to make an ink spot on the slide with a laboratory marker that can be used to unambiguously identify the focal plane of the top surface of the glass (note the cells themselves serve this purpose in the Petri dish). The stepper motor can then be used to lower the AFM scanner until the probe is just out of focus, bringing it close to the surface without accidentally bumping into it and breaking the AFM probe or damaging the scanner.
9. According to classical elasticity theory *(62)*, for a simple cantilever beam with a thin rectangular cross-section, the spring constant relating a point force at the end of the beam to its maximum deflection is given by $\kappa = Et^3w/4L^3$, where w is the width, L is the length, t is the thickness, and E is the elastic Young's modulus of the beam material. This basic formula has been modified to correct for the fact that the silicon nitride AFM probes commonly used for cell mechanics applications typically have a more complicated V- or A-shaped geometry and that the load on the probe tip is not applied exactly at the end of the cantilever *(63,64)*. However, the greatest limitation when using such formulas is uncertainty in the values of E and t (especially because of the strong nonlinear dependence on t), which are inherently imprecise as a result of the vapor-deposition process used in fabricating wafers of AFM probes *(57,59)*. Although variability in the spring constant of cantilevers from a given wafer is typically about 10% *(40,60)*, measured values of κ can vary by 50% or more between wafers and can differ substantially from nominal values supplied by the manufacturer *(40,60,65)*, necessitating calibration for accurate force measurements.
10. When the AFM is temporarily moved out of a liquid bath, as when exchanging samples, it sometimes happens that the voltage signal on the photodetector suddenly drops very low. Do not readjust the laser! This can occur when the volume of fluid on the scanner tip is small enough that the cantilever itself becomes bent by the

surface tension of the drop, so the laser reflection moves off the photodetector. When the voltage on the photodetector falls below some minimum value, software-controlled lowering of the AFM is prevented in order to protect the probe and scanner from accidentally contacting a surface undetected. To increase the photodetector signal and restore software control of the scanner position, the user must increase the volume of fluid on the scanner tip, either by manually lifting a dish of liquid up into contact with the scanner tip or by adding a few drops of liquid onto the scanner using the 3-mL syringe and 30G needle. When the cantilever is released from the surface tension of the drop, the photodetector signal will suddenly be restored.

11. Accurately engaging the tip of the AFM probe at a particular location on a sample can be challenging, even with the aid of a light microscope. However, this process can be greatly simplified when the microscope is equipped with a video camera and monitor. First, focus on the sample and use the stepper motor to bring the AFM within a few hundred micrometers of the sample. Next, adjust the microscope focus so the tip of the AFM probe comes clearly into focus on the video monitor. Mark the exact location of the probe tip on the monitor using the adhesive corner of a small Post-it note. Focus back on the sample and use the microscope's *x-y* stage to position the sample so the region of interest coincides with the tip location marked on the video monitor. Proceed to engage the AFM tip, which will slowly come into focus at the exact location marked on the video monitor, and hence at the desired location on the sample.
12. Standard silicon nitride AFM probes have a four-sided pyramidal tip geometry, with an inclination angle relative to the cantilever of 54.7°, defined by the crystal structure of the etched silicon molds on which they are fabricated *(57,66)*. The tip of the pyramid is not an ideal point, but, instead, has a variably blunted profile *(66,67)* that can be approximated as a sector of a sphere. Some investigators have attached glass or polystyrene microspheres to AFM probes to obtain a simplified tip geometry *(68–70)*, but this decreases spatial resolution and requires additional technical expertise. Custom probe modification can also be performed by some commercial vendors (e.g., Novascan Technologies, Ames, IA).
13. For accurate interpretation of indentation data, it is necessary for the cell to remain stationary during the measurement. Although typically not a problem for cells attached to a substrate, this becomes an issue for studying cells in suspension, as they tend to roll or move during indentation. In such cases, it might be possible to allow the cell to incubate for a brief period to initiate attachment, to use a non-specific binding agent such as poly-L-lysine (cat. no. P4707, Sigma, St. Louis, MO) to secure the cell to the substrate, or to use a micropipet or other device to hold the cell in place during the indentation experiment.
14. Adhesion between the AFM probe and the cell might be observed as negative deflections during probe retraction, especially near the point of initial contact with the cell. However, by the time the probe reaches its fully retracted position, the retraction curve should coincide with the flat precontact region of the advance curve. Sometimes long-range adhesion between the cell and the probe can be observed as downward deflection at the start of the advance curve and the end of the retract

curve. If this occurs, the user should extend the *z*-range or back up the tip (withdrawing completely if necessary) until the precontact region becomes flat again.

15. It is important to inspect the probe tip regularly under the microscope to ensure that no debris has accumulated on the probe. If contamination is suspected, withdraw the AFM and perform indentations on a clean glass slide (as described in **steps 7** and **8** in **Subheading 3.1.**) to ensure that the tip is clean and the postcontact curve is linear with unity slope. If this is not the case, the probe can sometimes be cleaned by removing the scanner and carefully rinsing the probe with fresh liquid using the 3-mL syringe and 30G needle or by carefully drying off the probe holder (without removing it from the scanner) with the corner of a Kimwipe® or cotton swab and gentle compressed air and rewetting the probe. Check the photodetector sensitivity (*see* **Subheading 3.1.**) to make sure that the laser and probe alignment have not changed during this process; if they have, simply record the new sensitivity and proceed with experiments.
16. Because cell height can vary by several micrometers over such large regions, it might be helpful to acquire force curves using a "trigger mode," in which the probe position is automatically adjusted to achieve a set maximum deflection (usually relative to the initial precontact deflection) for each indentation. This helps ensure consistency of force curves over a highly variable sample and also minimizes cell damage from excessively deep indentations on higher parts of the cell, although softer parts must be indented more deeply to achieve a given trigger deflection. For such applications, it is advantageous to have a scanner with an extended *z*-range of at least 10 μm.
17. Tapping mode imaging (in which feedback is used to maintain a constant amplitude of oscillation of the probe tip) is also well suited for imaging delicate samples such as cells ***(71)***. However, switching between tapping mode and force mode for indentations requires resetting of a number of control parameters. "Phase imaging" is a form of tapping mode in which changes in the phase of the tip oscillation relative to the probe input signal are interpreted to reflect the viscoelastic properties of the cell ***(72,73)***. One advantage of this technique is a rapid scan time (about 4 min for a 128 × 128 pixel image), but the physical interpretation of the data remains unclear and the resulting map is primarily of qualitative value.
18. A number of studies have documented stability and viability of cultured cells during contact mode imaging ***(4,65,74)***. However, it is also quite possible to damage a cell during this process ***(55,75,76)***. Therefore, it is advisable to perform a few test images for a given cell type and AFM probe to determine the best values of the most important scan parameters. In general, cells are more easily damaged at higher contact forces, so the set-point reference voltage should be decreased to the minimum value that still provides an acceptable image. Higher tip velocities also tend to cause damage, which means that a lower scan rate (in Hz) should be used with a larger scan size. It can be helpful to adjust the scan angle so that the fast-scan direction coincides with the direction of least change in cell height, such as moving along the length of actin stress fibers rather than repeatedly traversing the fibers to minimize disruption. A pixel resolution of 128 or 256 scan lines is often

adequate to visualize features of interest without unnecessarily lengthy scan times. Finally, a simple method to estimate the desired scan size on a particular cell without trial-and-error adjustments while scanning the cell is as follows. Immediately after engaging on the cell, use the stepper motor to back up the AFM probe about 10–20 μm out of contact with the cell while the software is still "engaged." Then increase the scan size until the probe is visibly moving over the region of the cell you wish to scan; again, Post-it® notes placed on a video monitor can help with this process. An AFM image will not be obtained during this time, of course, because the probe is not in contact with the cell. Once the scan size is determined, the probe can again be engaged on the cell to obtain a contact mode image with minimal further parameter adjustment.

19. In recognition of the limitations of the Hertz model for cell mechanics applications, a number of alternate approaches for analyzing AFM indentation data have also been developed. The method of force integration to equal limits overcomes several practical difficulties with standard AFM indentation, such as contact point uncertainty, to yield regional maps of relative cell stiffness *(28)*, but the analysis is ultimately founded on the same assumptions as the Hertz model. Dimitriadis et al. have recently developed an analytic correction for the Hertz model when applied to very thin samples, such as cells *(51)*. McElfresh and co-workers developed an analysis that explicitly accounts for surface interactions with the cell membrane for AFM indentation of sperm cells, but the approach makes other assumptions, such as single-point contact, that limit applicability to more general cell types *(77)*. In AFM "force modulation," small perturbations are applied upon a larger indentation *(78)*, for which Mahaffy and co-workers have recently developed a theoretical framework for extracting quantitative frequency-dependent elastic and viscous moduli of biological cells *(38,68)*.
20. The Hertz equation for a simple ideal cone is readily obtained for the case $b = 0$. However, it must be emphasized that ignoring (or underestimating) the blunt tip defect will result in overestimation of the elastic modulus, especially when based on data from the early response at small indentation depths *(37,53)*.
21. The standard approach is to perform a least squares fit of the general Hertz contact equation to the measured force–depth data set and extract a single value of $\widetilde{E}$ (or a related modulus) from each indentation test. This might be reasonable if the cell truly behaves like a simple linear elastic material (i.e., if the pointwise modulus, $\widetilde{E}_i$, is indeed independent of indentation depth). However, if the cell is actually a nonlinear material, then such a fitting procedure can lead to gross errors in the estimated value of elastic modulus *(37)*. Other attempts to determine a depth-dependent modulus have been made by fitting subsets of the postcontact data *(35,79)*. However, the resulting values of elastic modulus are difficult to interpret because the estimated contact point was also allowed to vary.

Acknowledgment

This work was funded in part by a CAREER Award from the NSF (BES-0239138).

References

1. Zhu, C., Bao, G., and Wang, N. (2000) Cell mechanics: Mechanical response, cell adhesion, and molecular deformation. *Annu. Rev. Biomed. Eng.* **2,** 189–226.
2. Elson, E. L. (1988) Cellular mechanics as an indicator of cytoskeletal structure and function. *Annu. Rev. Biophys. Biophys. Chem.* **17,** 397–430.
3. Pourati, J., Maniotis, A., Spiegel, D., et al. (1998) Is cytoskeletal tension a major determinant of cell deformability in adherent endothelial cells? *Am. J. Physiol.* **247,** C1283–C1289.
4. Rotsch, C. and Radmacher, M. (2000) Drug-induced changes of cytoskeletal structure and mechanics in fibroblasts: an atomic force microscopy study. *Biophys. J.* **78,** 520–535.
5. Trickey, W. R., Vail, T. P., and Guilak, F. (2004) The role of the cytoskeleton in the viscoelastic properties of human articular chondrocytes. *J. Orthop. Res.* **22,** 131–139.
6. Heidemann, S. R., Kaech, S., Buxbaum, R. E., and Matus, A. (1999) Direct observations of the mechanical behaviors of the cytoskeleton in living fibroblasts. *J. Cell Biol.* **145,** 109–122.
7. Sato, M., Nagayama, K., Kataoka, N., Sasaki, M., and Hane, K. (2000) Local mechanical properties measured by atomic force microscopy for cultured bovine endothelial cells exposed to shear stress. *J. Biomech.* **33,** 127–135.
8. Costa, K. D., Lee, E. J., and Holmes, J. W. (2003) Creating alignment and anisotropy in engineered heart tissue: role of boundary conditions in a model three-dimensional culture system. *Tissue Eng.* **9,** 567–577.
9. Wakatsuki, T. and Elson, E. L. (2003) Reciprocal interactions between cells and extracellular matrix during remodeling of tissue constructs. *Biophys. Chem.* **100,** 593–605.
10. Swartz, M. A., Tschumperlin, D. J., Kamm, R. D., and Drazen, J. M. (2001) Mechanical stress is communicated between different cell types to elicit matrix remodeling. *Proc. Natl. Acad. Sci. USA* **98,** 6180–6185.
11. Tamariz, E. and Grinnell, F. (2002) Modulation of fibroblast morphology and adhesion during collagen matrix remodeling. *Mol. Biol. Cell* **13,** 3915–3929.
12. Harris, A. K. (1994) Multicellular mechanics in the creation of anatomical structures, in Biomechanics of Active Movement and Division of Cells, *Volume H-84* (Akkas, N., ed.), Springer-Verlag, Berlin, pp. 87–129.
13. Costa, K. D. (2004) Single-cell elastography: probing for disease with the atomic force microscope. *Dis. Markers* **19,** 139–154.
14. Hochmuth, R. M. and Waugh, R. E. (1987) Erythrocyte membrane elasticity and viscosity. *Annu. Rev. Physiol.* **49,** 209–219.
15. Schmid-Schonbein, G. W., Sung, K. -L. P., Tozeren, H., Skalak, R., and Chien, S. (1981) Passive mechanical properties of human leukocytes. *Biophys. J.* **36,** 243–256.
16. Evans, E. and Yeung, A. (1989) Apparent viscosity and cortical tension of blood granulocytes determined by micropipet aspiration. *Biophys. J.* **56,** 151–160.
17. Jones, W. R., Ting-Beall, H. P., Lee, G. M., Kelley, S. S., Hochmuth, R. M., and Guilak, F. (1999) Alterations in the Young's modulus and volumetric properties of

chondrocytes isolated from normal and osteoarthritic human cartilage. *J. Biomech*. **32,** 119–127.
18. Miyazaki, H., Hasegawa, Y., and Hayashi, K. (2000) A newly designed tensile tester for cells and its application to fibroblasts. *J. Biomech*. **33,** 97–104.
19. Wang, N., Butler, J. P., and Ingber, D. E. (1993) Mechanotransduction across the cell surface and through the cytoskeleton. *Science* **260,** 1124–1127.
20. Yamada, S., Wirtz, D., and Kuo, S. C. (2000) Mechanics of living cells measured by laser tracking microrheology. *Biophys. J*. **78,** 1736–1747.
21. Alenghat, F. J., Fabry, B., Tsai, K. Y., Goldmann, W. H., and Ingber, D. E. (2000) Analysis of cell mechanics in single vinculin-deficient cells using a magnetic tweezer. *Biochem. Biophys. Res. Commun*. **277,** 93–99.
22. Guck, J., Ananthakrishnan, R., Mahmood, H., Moon, T. J., Cunningham, C. C., and Kas, J. (2001) The optical stretcher: a novel laser tool to micromanipulate cells. *Biophys. J*. **81,** 767–784.
23. Petersen, N. O., McConnaughey, W. B., and Elson, E. L. (1982) Dependence of locally measured cellular deformability on position on the cell, temperature, and cytochalasin B. *Proc. Natl. Acad. Sci. USA* **79,** 5327–5331.
24. Felder, S. and Elson, E. L. (1990) Mechanics of fibroblast locomotion: quantitative analysis of forces and motion at the leading lamellas of fibroblasts. *J. Cell Biol*. **111,** 2513–2526.
25. Koay, E. J., Shieh, A. C., and Athanasiou, K. A. (2003) Creep indentation of single cells. *J. Biomech. Eng*. **125,** 334–341.
26. Binnig, G., Quate, C. F., and Gerber, C. (1986) Atomic force microscope. *Phys. Rev. Lett*. **56,** 930–933.
27. Radmacher, M. (2002) Measuring the elastic properties of living cells by the atomic force microscope. *Methods Cell Biol*. **68,** 67–90.
28. A-Hassan, E., Heinz, W. F., Antonik, M. D., et al. (1998) Relative microelastic mapping of living cells by atomic force microscopy. *Biophys. J*. **74,** 1564–1578.
29. Butt, H. -J. and Jaschke, M. (1995) Calculation of thermal noise in atomic force microscopy. *Nanotechnology* **6,** 1–7.
30. Lehenkari, P. P., Charras, G. T., Nykanen, A., and Horton, M. A. (2000) Adapting atomic force microscopy for cell biology. *Ultramicroscopy* **82,** 289–295.
31. Lekka, M., Laidler, P., Gil, D., Lekki, J., Stachura, Z., and Hrynkiewicz, A. Z. (1999) Elasticity of normal and cancerous human bladder cells studied by scanning force microscopy. *Eur. Biophys. J*. **28,** 312–316.
32. Matzke, R., Jacobson, K., and Radmacher, M. (2001) Direct, high-resolution measurement of furrow stiffening during division of adherent cells. *Nature Cell Biol*. **3,** 607–610.
33. Mathur, A. B., Collinsworth, A. M., Reichert, W. M., Kraus, W. E., and Truskey, G. A. (2001) Endothelial, cardiac muscle and skeletal muscle exhibit different viscous and elastic properties as determined by atomic force microscopy. *J. Biomech*. **34,** 1545–1553.
34. Charras, G. T., Lehenkari, P. P., and Horton, M. A. (2001) Atomic force microscopy can be used to mechanically stimulate osteoblasts and evaluate cellular strain distributions. *Ultramicroscopy* **86,** 85–95.

35. Rotsch, C., Jacobson, K., and Radmacher, M. (1999) Dimensional and mechanical dynamics of active and stable edges in motile fibroblasts investigated by using atomic force microscopy. *Proc. Natl. Acad. Sci. USA* **96,** 921–926.
36. Domke, J., Parak, W. J., George, M., Gaub, H. E., and Radmacher, M. (1999) Mapping the mechanical pulse of single cardiomyocytes with the atomic force microscope. *Eur. Biophys. J*. **28,** 179–186.
37. Costa, K. D. and Yin, F. C. (1999) Analysis of indentation: implications for measuring mechanical properties with atomic force microscopy. *J. Biomech. Eng*. **121,** 462–471.
38. Mahaffy, R. E., Shih, C. K., MacKintosh, F. C., and Kas, J. (2000) Scanning probe-based frequency-dependent microrheology of polymer gels and biological cells. *Phys. Rev. Lett*. **85,** 880–883.
39. Mathur, A. B., Truskey, G. A., and Reichert, W. M. (2000) Atomic force and total internal reflection fluorescence microscopy for the study of force transmission in endothelial cells. *Biophys. J*. **78,** 1725–1735.
40. Cleveland, J. P., Manne, S., Bocek, D., and Hansma, P. K. (1993) A nondestructive method for determining the spring constant of cantilevers for scanning force microscopy. *Rev. Sci. Instrum*. **64,** 403–405.
41. Sader, J. E., Larson, I., Mulvaney, P., and White, L. R. (1995) Method for the calibration of atomic force microscope cantilevers. *Rev. Sci. Instrum*. **66,** 3789–3798.
42. Sader, J. E., Chon, J. W. M., and Mulvaney, P. (1999) Calibration of rectangular atomic force microscope cantilevers. *Rev. Sci. Instrum*. **70,** 3967–3969.
43. Ruan, J. -A. and Bhushan, B. (1994) Atomic-scale friction measurements using friction force microscopy: Part I—General principles and new measurement techniques. *ASME J. Tribol*. **116,** 378–388.
44. Tortonese, M. and Kirk, M. (1997) Characterization of application specific probes for SPMs. *Micromach. Imag. SPIE* **3009,** 53–60.
45. Jensen, F. (1993) Z calibration of the atomic force microscope by means of a pyramidal tip. *Rev. Sci. Instrum*. **64,** 2595–2597.
46. Heinz, W. F. and Hoh, J. H. (1999) Spatially resolved force spectroscopy of biological surfaces using the atomic force microscope. *Trends Biotechnol*. **17,** 143–150.
47. Weisenhorn, A. L., Khorsandi, M., Kasas, S., Gotzos, V., and Butt, H. -J. (1993) Deformation and height anomaly of soft surfaces studied with an AFM. *Nanotechniques* **4,** 106–113.
48. Sneddon, I. N. (1965) The relation between load and penetration in the axisymmetric Boussinesq problem for a punch of arbitrary profile. *Int. J. Eng. Sci*. **3,** 47–57.
49. Johnson, K. L. (1985) Contact Mechanics, Cambridge University Press, New York.
50. Domke, J. and Radmacher, M. (1998) Measuring the elastic properties of thin polymer films with the atomic force microscope. *Langmuir* **14,** 3320–3325.
51. Dimitriadis, E. K., Horkay, F., Maresca, J., Kachar, B., and Chadwick, R. S. (2002) Determination of elastic moduli of thin layers of soft material using the atomic force microscope. *Biophys. J.* **82,** 2798–2810.
52. Press, W. H., Teukolsky, S. A., Vetterling, W. T., and Flannery, B. P. (1992) *Numerical Recipes in FORTRAN 77: The Art of Scientific Computing*, Cambridge University Press, New York.

53. Briscoe, B. J., Sebastian, K. S., and Adams, M. J. (1994) The effect of indenter geometry on the elastic response to indentation. *J. Phys. D: Appl. Phys*. **27,** 1156–1162.
54. Hoh, J. H. and Schoenenberger, C. -A. (1994) Surface morphology and mechanical properties of MDCK monolayers by atomic force microscopy. *J. Cell Sci*. **107,** 1105–1114.
55. Schaus, S. S. and Henderson, E. R. (1997) Cell viability and probe–cell membrane interactions of XR1 glial cells imaged by atomic force microscopy. *Biophys. J*. **73,** 1205–1214.
56. Haydon, P. G., Lartius, R., Parpura, V., and Marchese-Ragona, S. P. (1996) Membrane deformation of living glial cells using atomic force microscopy. *J. Microsc*. **182,** 114–120.
57. Albrecht, T. R., Akamine, S., Carver, T. E., and Quate, C. F. (1990) Microfabrication of cantilever styli for the atomic force microscope. *J. Vac. Sci. Technol. A* **8,** 3386–3396.
58. Tortonese, M. (1997) Cantilevers and tips for atomic force microscopy. *IEEE Eng. Med. Biol. Mag*. **16,** 28–33.
59. Weisenhorn, A. L., Maivald, P., Butt, H. -J., and Hansma, P. K. (1992) Measuring adhesion, attraction, and repulsion between surfaces in liquids with an atomic force microscope. *Phys. Rev. B* **45,** 11,226–11,232.
60. Senden, T. J. and Ducker, W. A. (1994) Experimental determination of spring constants in atomic force microscopy. *Langmuir* **10,** 1003–1004.
61. Horton, M. A., Charras, G., Ballestrem, C., and Lehenkari, P. (2000) Integration of atomic force and confocal microscopy. *Single Mol*. **1,** 135–137.
62. Landau, L. D. and Lifshitz, E. M. (1970) *Theory of Elasticity,* Pergamon, Oxford.
63. Sader, J. E. and White, L. (1993) Theoretical analysis of the static deflection of plates for atomic force microscope applications. *J. Appl. Phys*. **74,** 1–9.
64. Sader, J. E. (1995) Parallel beam approximation for V-shaped atomic force microscope cantilevers. *Rev. Sci. Instrum.* **66,** 4583–4587.
65. Le Grimellec, C., Lesniewska, E., Giocondi, M. C., Finot, E., Vie, V., and Goudonnet, J. P. (1998) Imaging of the surface of living cells by low-force contact-mode atomic force microscopy. *Biophys. J*. **75,** 695–703.
66. Schwarz, U. D., Haefke, H., Reimann, P., and Güntherodt, H. J. (1994) Tip artefacts in scanning force microscopy. *J. Microsc*. **173,** 183–197.
67. Grütter, P., Zimmermann-Edling, W., and Brodbeck, D. (1992) Tip artifacts of microfabricated force sensors for atomic force microscopy. *Appl. Phys. Lett*. **60,** 2741–2743.
68. Mahaffy, R. E., Park, S., Gerde, E., Kas, J., and Shih, C. K. (2004) Quantitative analysis of the viscoelastic properties of thin regions of fibroblasts using atomic force microscopy. *Biophys. J*. **86,** 1777–1793.
69. Charras, G., Lehenkari, P., and Horton, M. (2002) Biotechnological applications of atomic force microscopy. *Methods Cell Biol*. **68,** 171–191.
70. Benoit, M. (2002) Cell adhesion measured by force spectroscopy on living cells. *Methods Cell Biol*. **68,** 91–114.

71. Vie, V., Giocondi, M. C., Lesniewska, E., Finot, E., Goudonnet, J. P., and Le Grimellec, C. (2000) Tapping-mode atomic force microscopy on intact cells: optimal adjustment of tapping conditions by using the deflection signal. *Ultramicroscopy* **82,** 279–288.
72. Nagao, E. and Dvorak, J. A. (1999) Phase imaging by atomic force microscopy: analysis of living homoiothermic vertebrate cells. *Biophys. J*. **76,** 3289–3297.
73. Hansma, H. G., Kim, K. J., Laney, D. E., et al. (1997) Properties of biomolecules measured from atomic force microscope images: a review. *J. Struct. Biol.* **119,** 99–108.
74. Rotsch, C., Braet, F., Wisse, E., and Radmacher, M. (1997) AFM imaging and elasticity measurements on living rat liver macrophages. *Cell Biol. Int*. **21,** 685–696.
75. You, H. X., Lau, J. M., Zhang, S., and Yu, L. (2000) Atomic force microscopy of living cells: a preliminary study of the disruptive effect of cantilever tip on cell morphology. *Ultramicroscopy* **82,** 297–305.
76. Braet, F., de Zanger, R., Seynaeve, C., Baekeland, M., and Wisse, E. (2001) A comparative atomic force microscopy study on living skin fibroblasts and liver endothelial cells. *J. Electron Microsc*. **50,** 283–290.
77. McElfresh, M., Baesu, E., Balhorn, R., Belak, J., Allen, M. J., and Rudd, R. E. (2002) Combining constitutive materials modeling with atomic force microscopy to understand the mechanical properties of living cells. *Proc. Natl. Acad. Sci. USA* **99(Suppl. 2),** 6493–6497.
78. Radmacher, M., Tillmann, R., and Gaub, H. (1993) Imaging viscoelasticity by force modulation with the atomic force microscope. *Biophys. J*. **64,** 735–742.
79. Radmacher, M., Fritz, M., Kacher, C. M., Cleveland, J. P., and Hansma, P. K. (1996) Measuring the viscoelastic properties of human platelets with the atomic force microscope. *Biophys. J*. **70,** 556–567.